IEEE Access
Multidisciplinary ⋮ Rapid Review ⋮ Open Access Journal

Received March 24, 2021, accepted April 14, 2021, date of publication April 20, 2021, date of current version April 29, 2021.

Digital Object Identifier 10.1109/ACCESS.2021.3074219

Surface Defect Detection of Solar Cells Based on Multiscale Region Proposal Fusion Network

XIONG ZHANG[1,2], TING HOU[2], YAWEN HAO[2], HONG SHANGGUAN[1,2], ANHONG WANG[2], AND SICHUN PENG[2]

[1]Shanxi Key Laboratory of Advanced Control and Equipment Intelligence, Taiyuan University of Science and Technology, Taiyuan 030024, China
[2]School of Electronic Information Engineering, Taiyuan University of Science and Technology, Taiyuan 030024, China

Corresponding author: Xiong Zhang (zx@tyust.edu.cn)

This work was supported in part by the Shanxi Key Laboratory of Advanced Control and Equipment Intelligence under Grant 201805D111001, in part by the Scientific and Technological Innovation Team of Shanxi Province under Grant 201705D131025, in part by the Collaborative Innovation Center of Internet + 3D Printing in Shanxi Province under Grant 201708, and in part by the Excellent Graduate Innovation Project of Shanxi Province under Grant 2019SY488.

ABSTRACT Manufacturing process and human operational errors may cause small-sized defects, such as cracks, over-welding, and black edges, on solar cell surfaces. These surface defects are subtle and, therefore, difficult to observe and detect. Accurate detection and replacement of defective battery modules is necessary to ensure the energy conversion efficiency of solar cells. To improve the adaptability to the scale changes of various types of surface defects of solar cells, this study proposed a multi-feature region proposal fusion network (MF-RPN) structure to detect surface defects. In such a network, region proposals are extracted from different feature layers of convolutional neural networks. Additionally, considering that multiple aspect ratios and scale settings and the use of multiple RPNs, result in an overlap of candidate regions and lead to information redundancy, we designed a multiscale region proposal selection strategy (MRPSS) to reduce the number of region proposals and improve network accuracy. Owing to the complete learning of shallow-detail texture information and deep semantic information, our multiscale RPN fusion structure can effectively improve an object's multiscale feature extraction ability for various scales and types of surface defects of solar cells. Experimental results demonstrate that our method outperforms other methods by achieving a higher detection accuracy.

INDEX TERMS Deep learning, defects detection, faster R-CNN, multiscale fusion, RPN, solar cell.

I. INTRODUCTION

Solar energy is a high-quality and environmentally friendly energy source that does not require fuel consumption. Usable solar energy is obtained from photovoltaic power generation systems, which are a typical emerging energy technology [1]–[3]. Widespread use of photovoltaic power generation technology is expected to alleviate the environmental problems caused by non-renewable energy sources, such as petroleum. However, certain factors decrease the power generation efficiency of photovoltaic modules and shorten their service life. These include the fragility of the solar wafer substrate, manufacturing process defects, and artificial misoperation, which causes hard-to-detect surface cracks, over-welding, black edges, unsoldered areas, and other subtle defects on the surface of solar cells. Therefore, detection methods that are advanced, precise, and yield fast results are an attractive but challenging research area for engineering purposes. Moreover, an in-depth study of the surface defect detection technology of solar cell modules [4], [5], especially their automatic classification and detection, is theoretically significant and invaluable in practical terms.

Currently, there are three main types of defect detection methods for solar cell surfaces: artificial visual, physical, and machine vision methods [6]–[8]. Among these, the defect detection method based on machine vision has attracted considerable developmental interest because of its many advantages, such as real-time detection, accuracy, speed, and operational convenience. From the perspective of mathematical modeling, surface defect detection algorithms are divided into image domain analysis (e.g., gradient feature [9], [10], clustering [11], [12], and matrix

The associate editor coordinating the review of this manuscript and approving it for publication was Juan Liu.

decomposition [13]), transform domain analysis (e.g., Fourier transform [14] and wavelet transform [8]), and deep learning methods [15], [16].

In 2012, Hinton and Salakhutdinov [17] proposed the use of a convolutional neural network (CNN) to extract features that are more robust and expressive, and CNNs are now widely used in computer vision. In 2013, Girshick *et al.* [18] proposed regions with convolutional neural network (R-CNN) features to introduce deep learning object detection. R-CNN uses a selection search algorithm to generate candidate regions of objects, CNN for feature extraction, support vector machine for convolutional feature classification, and linear regression for object detection. In 2015, Girshick [19] proposed the Fast R-CNN, as training the R-CNN was time-consuming, the test was slow and calculations were repeated. As GPUs lack high parallel computing capabilities, Fast R-CNN has a low detection efficiency and does not meet the needs of real-time applications. The Faster R-CNN [20] proposed by Ren *et al.* uses a shared convolutional network to form a region proposal network (RPN) to generate region proposals, thereby substantially improving the detection speed and accuracy. In 2017, Lin *et al.* proposed the FPN [21] network, which designed a pyramid-shaped multiscale feature structure to improve the network's ability to describe multiscale objects, and the performance of small object detection was greatly improved without increasing the calculation amount of the original model.

Inspired by the successful applications of deep learning, deep learning methods for detecting surface defects on solar cells are gradually advancing. Chen *et al.* [22] designed a visual defect detection method based on multispectral deep CNN, wherein the CNN model explores surface defect information in images of different spectral bands with enhanced recognition abilities for complex texture background and defect features. Several other efforts have also been reported in the literature, such as a deep learning-based classification pipeline structure [23] introduced to perform preprocessing (e.g., distortion correction, segmentation, and perspective correction on electro-luminescence images), a deep CNN designed for solar cell surface defect classification, and an investigation on the influence of a few oversamples and increase in data on system accuracy [24].

Generally, the surface defects of solar cells vary in shape and scale; hence, it is necessary to use different layers of neural network with different receptive fields to extract the optimal features of various types of defects. Therefore, a fixed convolutional layer cannot ensure that extracted features have sufficient validity. This study aimed to enhance the feature expression ability of the detection network for surface defect detection of solar cells of different shapes and scales. Thus, we proposed a multiscale RPN fusion network structure consisting of three RPN networks in different feature layers of the Faster R-CNN network structure. These RPN networks generate a certain proportion of region proposals for three sizes of defects, and all the obtained region proposals are selected by non-maximum suppression (NMS). The network structure was modified to use both low-level and high-level features for detection, thereby improving the network detection accuracy. Additionally, considering that multiple aspect ratios, scale settings, and the use of multiple RPNs cause a redundancy of suggested regions, we designed a multiscale region proposal selection strategy (MRPSS) to reduce the number of region proposals and improve the accuracy of the output prediction box.

II. METHODS

The surface defects of solar cells have diverse shapes and large-scale variations. Their processing requires features extracted from different receptive fields. Therefore, it is difficult to achieve desirable feature expression for diverse defects using the features output from a fixed convolutional layer. The Faster R-CNN is a classic algorithm among object detection deep learning algorithms, but it performs poorly when directly detecting the surface defects of solar cells because of the particularity of such defects.

To enhance the feature expression ability of the detection network for solar cell surface defects of different shapes and scales, we proposed a multiscale RPN fusion network structure. This network structure consists of three RPN networks in different feature layers of the Faster R-CNN network structure, to generate region proposals with a certain proportion of three defect sizes (i.e., large, medium, and small). The obtained candidate regions are fused and filtered before they are moved to the classification and regression module to obtain the category label and location of the defect.

A. OVERALL NETWORK STRUCTURE

The overall network structure based on multiscale RPN fusion proposed in this study (Fig. 1) comprises four parts: feature extraction module, multiscale RPN fusion module, region of interest (ROI) pooling layer, and classification regression module.

Feature extraction module (Part 1, Fig. 1): After the defect image to be analyzed is input to the network, it is extracted by five feature extraction units to obtain the main feature map of the defect image. Each feature extraction unit consists of convolutional layers, activation functions, and a pooling layer. To avoid the problem of gradient disappearance and degradation caused by the deepening of the network, the identity mapping of ResNet is introduced, and a cross-layer connection structure is adopted on the third, fourth, and fifth feature extraction units.

Multiscale RPN fusion module (Part 2, Fig. 1): The feature maps generated by the third, fourth, and fifth layers of the CNN are used as the inputs to three RPN modules. The candidate object regions are extracted from the feature maps at different scales, and the three scale region proposals are fused and filtered using the MRPSS strategy.

ROI pooling layer: The input of this layer includes not only the feature maps generated by the third, fourth, and fifth feature layers but also the region proposals generated by the multiscale RPN fusion module. The ROI pooling layer can

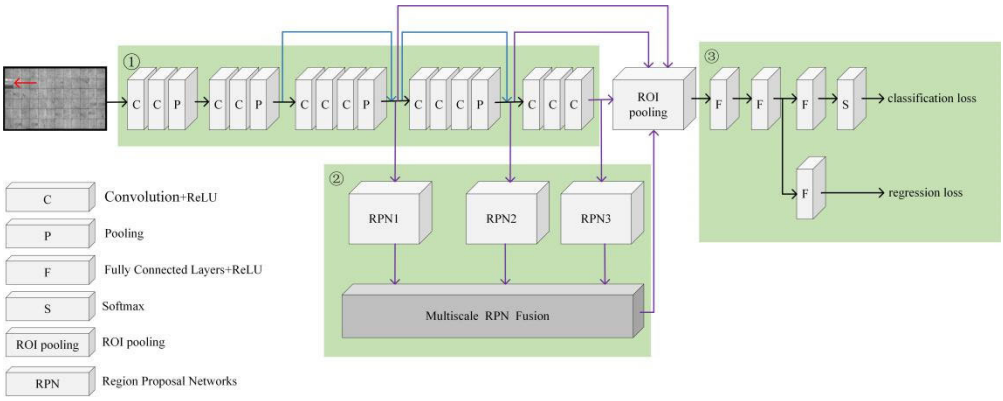

FIGURE 1. Overall network structure.

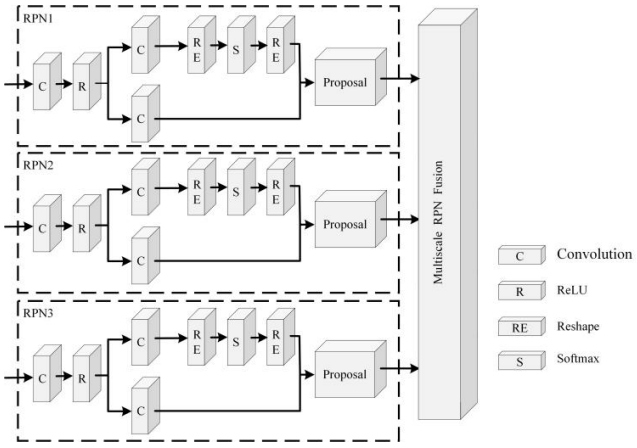

FIGURE 2. RPN structure.

convert inputs of different shapes into a vector feature output of a fixed length.

Classification regression module (Part 3, Fig. 1): The output of the ROI pooling layer is used as the input to this module, the category of the suggested region is calculated through the fully connected layer, and the bounding box regression algorithm is used to obtain the final position of the defects. In the whole process, the convolutional layer uses a 3×3 convolution kernel with a filling and step size of 1 each, and all pooling layers use a 2×2 convolution kernel with a step size of 2.

B. MULTISCALE RPN FUSION METHOD

Fig. 2 illustrates the RPN fusion network structure, and each RPN network contains two branches. The top branch uses the SoftMax classification rule to determine whether a region proposal contains an object, and the other branch calculates and obtains its location.

The proposal layer selects the suggested regions by eliminating those that are too small or beyond the boundary based on the information from the previous branches, and each region-generating network generates multiple ROIs. The algorithm uses the NMS method to eliminate redundant region proposals. First, sorting is performed according to the confidence score, and then the region proposal that acts as a positive sample corresponding to the highest confidence is selected. Other regions are traversed to calculate the intersection over union (IOU) between the current region and the positive sample, and the region proposals with an IOU value greater than the threshold are discarded. A region proposal with a relatively high confidence score is then obtained from the suggested regions with an IOU value less than the threshold, and the above steps are repeated until all regions are processed.

C. MRPSS

In the RPN, the extraction of region proposals in the multi-feature layer, and the multiscale and multi-aspect ratio setting of anchor points cause an overlapping of suggested regions and information redundancy on the same object. To reduce the overlap, a MRPSS strategy is used to filter the redundancies. In the training dataset, the defects with pixel dimensions less than 128×128, those with dimensions between 128×128 and 256×256, and those with dimensions larger than 256×256 are defined as small-, medium-, and large-sized defects, respectively. Fig. 3 illustrates the region proposal selection flowchart of RPN1. In the specific fusion selection method, as the region proposals in RPN1 are mainly used to detect small defects, the large region proposal is judged as invalid, and the ratio of the numbers of the reserved medium- to small-sized proposals is α:1-α. In RPN2, region proposals are only valid for medium-sized defects; therefore, small- and large-sized proposals are discarded. In RPN3, the region proposals are mainly for large- and medium-sized defects. At this point, the small-sized region proposals are discarded, and the ratio of the number of the reserved medium- to large-sized proposals is β:1-β. As the region proposals extracted from different feature layers have different receptive fields, adaptability to the changes in defect sizes is ensured.

D. EXPERIMENTAL ENVIRONMENT AND BASIC TRAINING PARAMETERS

In this study, we implemented the proposed networks on the Caffe deep learning framework. We collected pictures of

TABLE 1. Statistical information of pixel dimensions of defects on solar cell images.

Types	Small-sized defects	Medium-sized defects	Large-sized defects
Definition	Pixel dimensions < 128 × 128	128 × 128 < Pixel dimensions < 256 × 256	Pixels dimensions > 256 × 256
Number of images	289	839	333
Proportion in all defective images	0.198	0.574	0.228

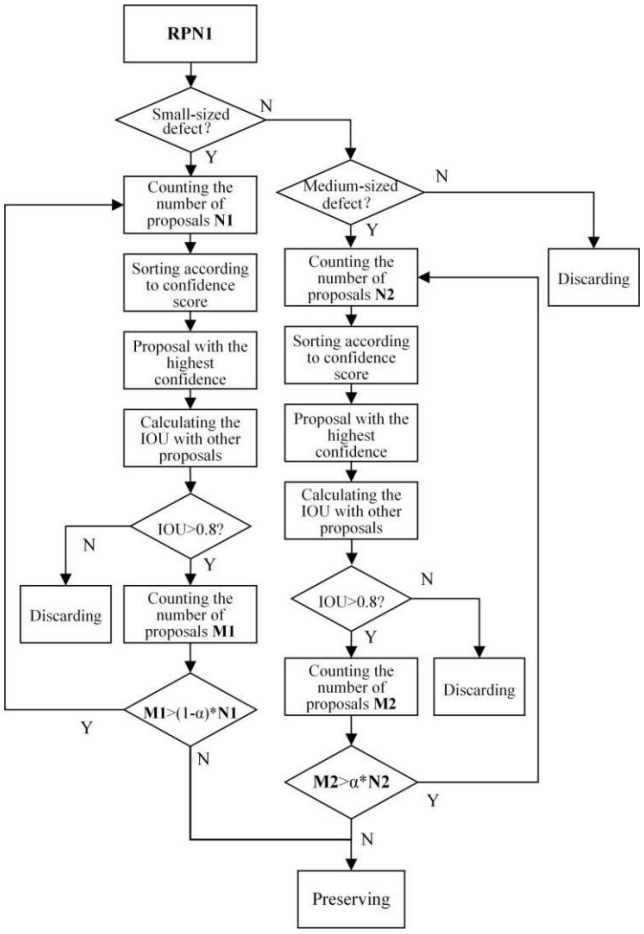

FIGURE 3. Multiscale region proposal selection strategy.

defective solar cells, calibrated the defect position manually by a Labelimg software, and produced a data set in accordance with the VOC2007 format. The training set contains 1461 solar cell surface images, and the test set contains 200 solar cell surface images. There are three types of defects: broken cell, crack and unsoldered. Moreover, to learn the defect characteristics, identify the defect types, and obtain the defect location, we trained the Faster R-CNN, R-FCN, FPN, YOLO series network, and the proposed network separately. In the training process, the number of iterations was set to 120,000; the learning rate was 0.01; and the weight attenuation and momentum factors were 0.0005 and 0.9 respectively [20]. In the testing phase, the outputs were the defect categories, regression position, and confidence of the bounding box.

1) FUSION FILTERING RELATED PARAMETERS

To select the appropriate fusion filtering parameters, we statistically analyzed the pixel dimensions of various defects in 1,461 solar cell images (as shown in Table 1). There are 1743 defects in total. The size of solar cell images in the data set is large and inconsistent. The resolution of solar cell images in the data set is 5320 × 2720, while the size of the defect area in the image is mostly in the range of 444 × 457. According to the statistical results of the size of defects in the training data set, the 345 defects with a pixel size smaller than 128 × 128 are defined as small-sized defects; and the 1000 defects with a pixel size between 128 × 128 and 256 × 256 are defined as medium-sized defects; and the 398 defects with a pixel size greater than 256 × 256 are defined as large-sized defects. The analysis demonstrated that the proportions of small-, medium-, and large-sized defects in the test images were 0.198, 0.574, and 0.228, respectively. In the RPN1 stage, the shallow network is more suitable for small-scale defect detection because of its smaller receptive field. In this experiment, α was set to 0.4, meaning the suggested regions having 60% small-sized and 40% medium-sized defects were reserved. In the RPN2 stage, the network is suitable for medium-sized defect detection; hence, we only reserved the suggested regions of medium-sized defects in the experiment. In the RPN3 stage, the deep network integrates semantic information more efficiently and has a larger receptive field, making it suitable for large-sized defect detection. In the experiment, β was set to 0.4, which implies that the suggested regions of 40% medium-sized and 60% large-sized defects were reserved. This setting ensures that the overall proportion of small, medium, and large sizes was 0.2:0.6:0.2, which is consistent with its prior distribution of 0.198:0.574:0.228.

2) ANCHOR-RELATED PARAMETERS

In the training set, some of the images contained a single defect, whereas some contained multiple defects, and each solar cell image contained a different number of defects. For cracks, broken cells, and unsoldered areas, using the 2562,

TABLE 2. Anchor point-related parameter statistics.

Setting	Anchor scales	Aspect ratios	mAP (%)
1 scale, 1 ratio	256	1:1	68.8
3 scale, 3 ratios	[128,256,512]	[1:1,1:2,2:1]	72.4
5 scale, 5 ratios	[32,64,128,256,512]	[1:1,1:2,1:3,3:1,2:1]	76.5

1:1 anchor point setting of the traditional Faster R-CNN enlarges the area of the most suggested bounding boxes compared to the actual defect area. Owing to the minute characteristics of the surface defects of solar cells, the anchor points may be easily misjudged as negative samples or irrelevant samples and get discarded. In this study, the size and proportion of the anchor points were changed according to the statistics of the pixel dimensions of the defects in the training set images. In the experiments, we re-set 25 (ratios $\times$ scale) anchor points. There were five types of ratios and five types of scales. Table 2 presents the statistics of specific parameters and mean average precision (mAP) values.

III. EXPERIMENTAL RESULTS AND ANALYSIS

We analyzed the performance of the proposed method in terms of the regression bounding box and classification accuracies. Fig. 4 illustrates the local enlarged images of the detection results of the same defect obtained using the proposed method and Faster R-CNN. It can be observed from Fig. 4 (a1 and a2) that a missed detection appears in the results of Faster R-CNN, and the crack location is not detected. However, our method accurately identified the crack location and obtained a confidence level of 0.99. As shown in Fig. 4 (b1 and b2), the proposed method obtained a higher confidence level, and the position of the regression bounding box is more accurate and without any missed detections. As also shown in Fig. 4 (c1 and c2), both methods detected the position of the unsoldered areas; however, the regression bounding box in the results of Faster R-CNN is larger with an expanded portion. Owing to the use of multiscale information, as well as the anchor point and aspect ratio suitable for the surface defects of solar cells, our algorithm performs better in terms of both the accuracy of the regression bounding box and the confidence level.

To further verify the effectiveness of the proposed method, we compared its detection results with those of several popular detection networks, such as YOLO, YOLO V2, YOLO V3, Faster R-CNN, R-FCN, and FPN. Figs. 5–7 illustrate the detection results of broken cells, crack, and unsoldered areas, respectively, using different detection networks. It can be also observed that the series of YOLO networks shows poor regression accuracy, and the detection regression accuracies are in the following order: YOLO $<$ YOLO V2 $<$ YOLO V3 $<$ Faster R-CNN $<$ R-FCN $<$ FPN $<$ proposed method. The regression accuracies of our method were higher than those of other networks.

Additionally, we analyzed the quantitative performance of different detection results. Tables III summarize the defect detection results of different methods. As shown in Table 3, compared to Faster R-CNN, the detection accuracy of our method is improved because of the effective fusion of shallow and deep features. Moreover, the false-positive (FPR) and false-negative rates (FNR) are significantly reduced. Particularly, the number of false-positive (FP) images is significantly reduced. The number of false-positive (FP) crack images detected using Faster R-CNN and our method are 16 and 4, respectively. The number of false-positive (FP) broken cell images and false-positive (FP) unsoldered cell images detected using Faster R-CNN are 9 and 21, respectively, and the number of false-positive (FP) images detected using our method is 3. Moreover, it can be observed from Table 3 that the accurate detection rate of our method is higher, while the false-positive (FPR) and false-negative rates(FNR) are significantly decreased. Compared to Faster R-CNN, the comprehensive accuracy of our method for the three defects is improved by 6.5%. This shows that the multiscale features and multi-anchor points in our method enhance the detection effect, especially for the detection of ultra-small defects on solar cell surfaces.

In the experiment, we also analyzed the mAP value performance of the detection results of different algorithms. As shown in Table 4, YOLO unifies the multistage detection into a simple neural network, and the detection speed is fast. However, YOLO is not suitable for the detection of surface defects of solar cells, and its defect detection mAP value is low. YOLO V9000 and YOLO V3 are improved versions of YOLO. Their detection accuracies are improved, but their detection effects are inferior to our method. It can be observed from Table 4 that the detection accuracy of our method is improved by more than 2.5% compared to other algorithms.

To analyze the effect of the multiscale RPN fusion method, we examined the performance of region proposals before and after the operations of MRPSS. Generally, when there are a few region proposals left in the region proposals selection stage, the regression accuracy of defects detection is low. However, too many calculations are encountered when there are too many region proposals left. To effectively solve and mitigate the increase in region proposals caused by a multi-anchor and multi-RPN fusion structure, we first used the NMS algorithm to remove a few redundant region proposals in each RPN. The region proposals selection strategy was then used to filter all region proposals for a second time. Figs. 8 and 9 show the schematics of the positions of region proposals before and after the NMS algorithm application, and the MRPSS strategy, respectively. It can be observed that some redundant region proposals can be removed using the fusion algorithm, further reducing the computational burden. To evaluate the real-time performance of the proposed algorithm, we measured the time taken to

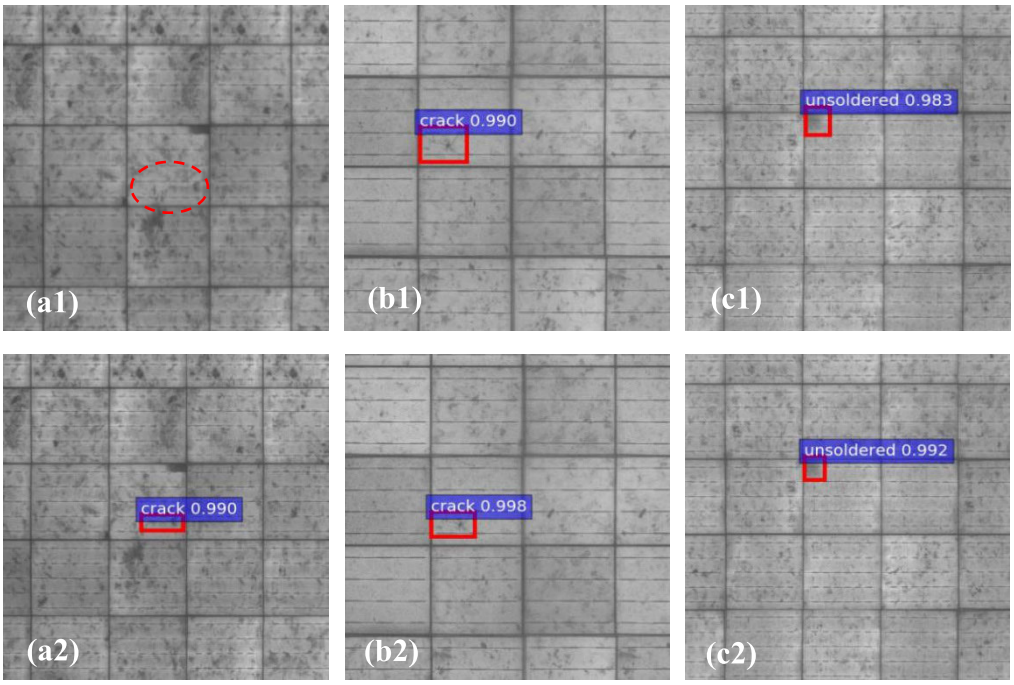

FIGURE 4. Partially enlarged images of the defect detection results obtained using Faster R-CNN and the proposed method.

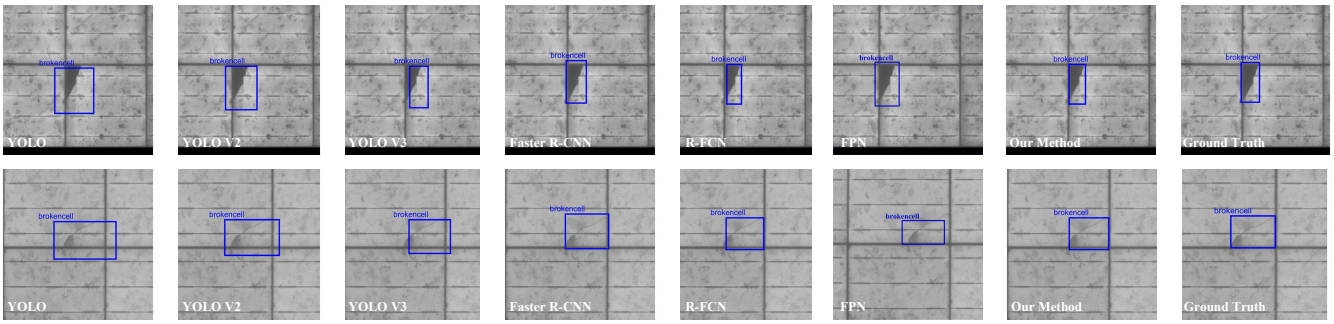

FIGURE 5. Partially enlarged images of the bounding box for broken cells of different defect models.

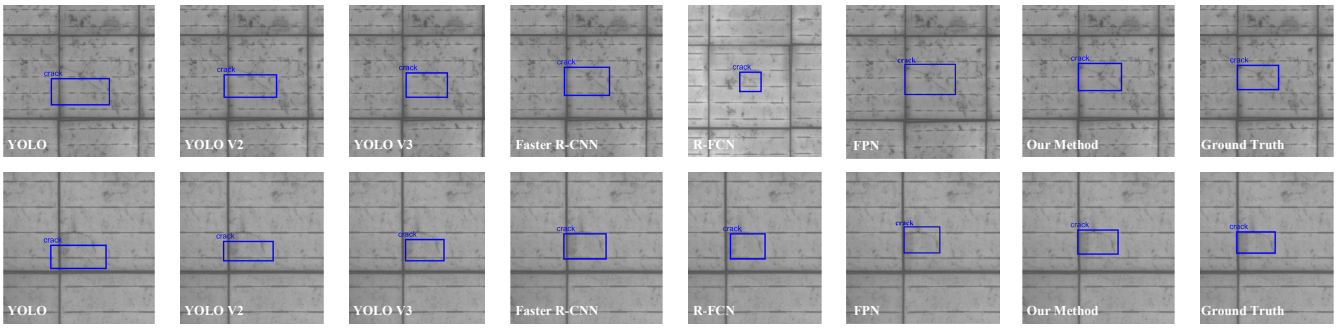

FIGURE 6. Partially enlarged images of the bounding box for cracks of different defect models.

test 600 defective solar cell images using Faster R-CNN, Faster R-CNN with improved anchor points, and our method. As shown in Table 5, the proposed multiscale detection algorithm requires a longer average detection time and has a poor real-time performance compared to the other algorithms. In summary, while improving the accuracy of the regression

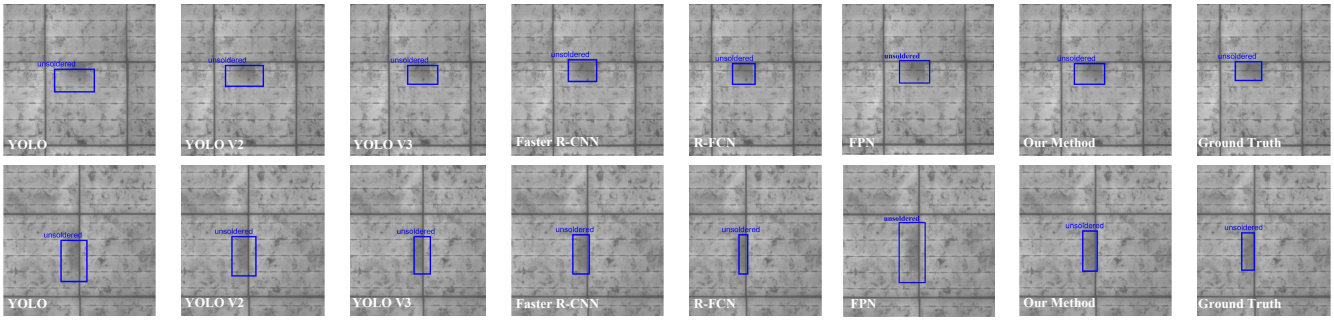

FIGURE 7. Partially enlarged images of the bounding box for unsoldered areas of different defect models.

TABLE 3. The statistics of different detection results.

		Broken cell	Crack	Unsoldered area	Total number
Faster R-CNN	Accurate	190	179	170	548
	FN	1	5	0	6
	FP	9	16	21	46
Our method	Accurate	196	194	197	587
	FN	1	2	0	3
	FP	3	4	3	10
Faster R-CNN(%)	Accuracy	0.950	0.895	0.895	0.913
	FNR	0.005	0.025	0	0.010
	FPR	0.045	0.080	0.105	0.077
Our method(%)	Accuracy	0.980	0.970	0.985	0.978
	FNR	0.005	0.010	0	0.005
	FPR	0.015	0.020	0.015	0.017

TABLE 4. mAP values of different methods.

Method	mAP (%)
YOLO	74.2
YOLO V9000	79.7
YOLO V3	80.1
Faster R-CNN	82.5
R-FCN	83.6
FPN	84.2
Our Method	85.0

TABLE 5. Test times of different algorithms.

	Total test time (s)	Average test time (s/piece)
Faster R-CNN	254.146	0.424
Faster R-CNN (multi-anchor)	270.817	0.451
Our Method	568.617	0.947

bounding box, the calculation amount of our method did not increase substantially, but the detection speed is sufficient for practical applications.

TABLE 6. The statistical results of ablation experiments.

Method	MF-RPN	MRPSS	mAP (%)
Faster R-CNN			82.5
Our method+	√		84.4
Our method++	√	√	85.0

Finally, in order to further explore the reliability of the proposed method and evaluate the effectiveness of MF-RPN and MRPSS, we performed ablation experiments. Respectively, we trained our method^{+} which adding only MF-RPN into the backbone Faster R-CNN and our method^{++} which adding both MF-RPN and MRPSS into the backbone Faster R-CNN on the dataset, and analyzed the test results obtained by different strategies. Table 6 shows the statistical results of mAP values obtained by different strategies. As can be seen from the table, our method^{++} achieved the highest mAP. With the addition of MF-RPN, our method^{+} obtained an mAP value which is not only 1.9% higher than that of Faster R-CNN, but also 0.2% higher than that of FPN. With the addition of MF-RPN and MRPSS, our method^{++} obtained a considerable mAP which can reach to 85.0% and increase

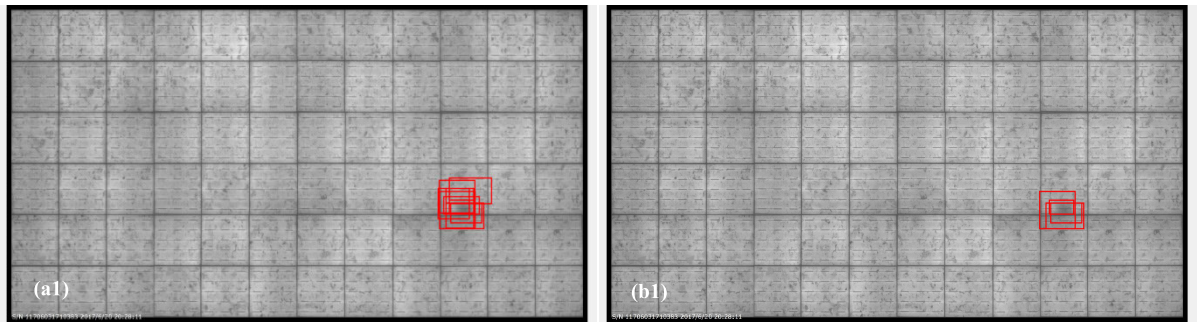

FIGURE 8. Schematic of region proposals before and after implementing the NMS algorithm.

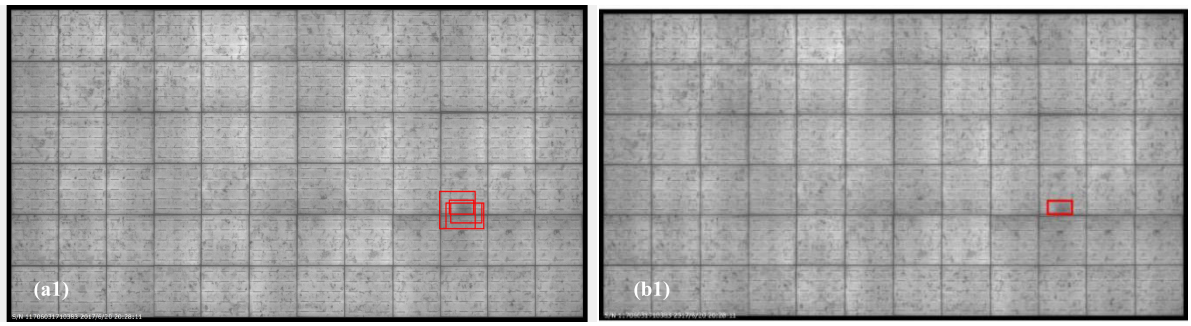

FIGURE 9. Schematic of suggested bounding box before and after fusion filtering.

by 2.5% over the original Faster R-CNN. In summary, the proposed method is effective on the detection of the solar cell surface defects.

IV. CONCLUSION

The detection of surface defects of solar cells contributes to the efficiency of solar cell generation and service life, and has attracted considerable research interest. The surface defects of solar cells vary widely both in shape and nature, and the classic deep learning object detection network, Faster R-CNN, has a poor detection accuracy. Hence, to improve the detection accuracy, we proposed a neural network model based on multiscale RPN fusion. Based on the original Faster R-CNN structure, the multiscale region proposals are extracted from different feature layers, and the selection and fusion strategy of multiscale region proposals improve the network's adaptability to changes in the shape and scale of detected objects. The experimental results demonstrated that our proposed network model has a lower probability of yielding false and missed detection for different types of defects compared to the latest deep learning object detection models. A limitation of this work is that the proposed network model requires a longer detection time than other methods. Hence, future studies should focus on reducing the detection time, simplifying the algorithm complexity, and improving the real-time application performance without compromising the detection accuracy.

REFERENCES

[1] Y. M. Zhang, "The current status and prospects of solar photovoltaic industry in China," *Energy Res. Utilization*, vol. 1, pp. 27–28, May 2007.

[2] (Jan. 15, 2016). *Yangzhou Sci-Tech & Information Research Institute: Development Status and Trend Analysis of Solar Photovoltaic Industry in China and Abroad in 2015 [N/OL]*. Accessed: Jun. 21, 2016. [Online]. Available: http://www.yzinfo.net.cn/yzinfo/qbck-2016.asp

[3] D. E. Sawyer and H. K. Kessler, "Laser scanning of solar cells for the display of cell operating characteristics and detection of cell defects," *IEEE Trans. Electron Devices*, vol. 27, no. 4, pp. 864–872, Apr. 1980.

[4] Q. Li, W. Wang, C. Ma, and Z. Zhu, "Detection of physical defects in solar cells by hyper spectral imaging technology," *Opt. Laser Technol.*, vol. 42, pp. 1010–1013, 2010.

[5] Y. H. Tsai, D. M. Tsai, and W. C. Li, "Defect detection of solar cells using EL imaging and Fourier image reconstruction," Tech. Rep., 2013.

[6] D.-M. Tsai, C.-C. Chang, and S.-M. Chao, "Micro-crack inspection in heterogeneously textured solar wafers using anisotropic diffusion," *Image Vis. Comput.*, vol. 28, no. 3, pp. 491–501, Mar. 2010.

[7] Q. Zou, Y. Cao, Q. Li, Q. Mao, and S. Wang, "CrackTree: Automatic crack detection from pavement images," *Pattern Recognit. Lett.*, vol. 33, no. 3, pp. 227–238, Feb. 2012.

[8] W.-C. Li and D.-M. Tsai, "Wavelet-based defect detection in solar wafer images with inhomogeneous texture," *Pattern Recognit.*, vol. 1, pp. 742–756, Aug. 2011.

[9] S. A. Anwar and M. Z. Abdullah, "Micro-crack detection of multicrystalline solar cells featuring an improved anisotropic diffusion filter and image segmentation technique," *EURASIP J. Image Video Process.*, vol. 2014, no. 1, pp. 1–17, Dec. 2014.

[10] S. Zhao, J. Zhao, Y. Wang, and X. Fu, "Moving object detecting using gradient information, three-frame-differencing and connectivity testing," in *Proc. Australas. Joint Conf. Artif. Intell.*, vol. 4304. Berlin, Germany: Springer, 2008, pp. 510–518.

[11] D.-M. Tsai, G.-N. Li, W.-C. Li, and W.-Y. Chiu, "Defect detection in multicrystal solar cells using clustering with uniformity measures," *Adv. Eng. Informat.*, vol. 29, no. 3, pp. 419–430, Aug. 2015.

[12] K. Agroui, M. Pellegrino, and F. Giovanni, "Analysis techniques for photovoltaic modules based on amorphous solar cells," *Arabian J. Sci. Eng.*, vol. 42, no. 1, pp. 375–381, Jan. 2017.

[13] C. Lu, J. Feng, Y. Chen, W. Liu, Z. Lin, and S. Yan, "Tensor robust principal component analysis: Exact recovery of corrupted low-rank tensors via convex optimization," in *Proc. IEEE Conf. Comput. Vis. Pattern Recognit. (CVPR)*, Vancouver, BC, Canada, Jun. 2016, pp. 2080–2088.

[14] D.-M. Tsai, S.-C. Wu, and W.-C. Li, "Defect detection of solar cells in electroluminescence images using Fourier image reconstruction," *Sol. Energy Mater. Sol. Cells*, vol. 99, pp. 250–262, Apr. 2012.
[15] F.-C. Chen and M. R. Jahanshahi, "NB-CNN: Deep learning-based crack detection using convolutional neural network and Naïve Bayes data fusion," *IEEE Trans. Ind. Electron.*, vol. 65, no. 5, pp. 4392–4400, May 2018.
[16] J. Schmidhuber, "Deep learning in neural networks: An overview," *Neural Netw.*, vol. 61, pp. 85–117, Jan. 2015.
[17] G. E. Hinton, "Reducing the dimensionality of data with neural networks," *Science*, vol. 313, no. 5786, pp. 504–507, Jul. 2006.
[18] R. Girshick, J. Donahue, T. Darrell, and J. Malik, "Rich feature hierarchies for accurate object detection and semantic segmentation," in *Proc. IEEE Conf. Comput. Vis. Pattern Recognit.*, Jun. 2014, pp. 580–587.
[19] R. Girshick, "Fast R-CNN," in *Proc. IEEE Int. Conf. Comput. Vis. (ICCV)*, Dec. 2015, pp. 1440–1448.
[20] S. Ren, K. He, R. Girshick, and J. Sun, "Faster R-CNN: Towards real-time object detection with region proposal networks," *IEEE Trans. Pattern Anal. Mach. Intell.*, vol. 39, no. 6, pp. 1137–1149, Jun. 2017.
[21] T.-Y. Lin, P. Dollar, R. Girshick, K. He, B. Hariharan, and S. Belongie, "Feature pyramid networks for object detection," in *Proc. IEEE Conf. Comput. Vis. Pattern Recognit. (CVPR)*, Jul. 2017, pp. 2117–2125.
[22] H. Chen, Y. Pang, Q. Hu, and K. Liu, "Solar cell surface defect inspection based on multispectral convolutional neural network," *J. Intell. Manuf.*, vol. 31, no. 2, pp. 453–468, Feb. 2020.
[23] T. Shanableh, "Saliency detection in MPEG and HEVC video using intra-frame and inter-frame distances," *Signal, Image Video Process.*, vol. 10, no. 4, pp. 703–709, Apr. 2016.
[24] M. W. Akram, G. Li, Y. Jin, X. Chen, C. Zhu, X. Zhao, A. Khaliq, M. Faheem, and A. Ahmad, "CNN based automatic detection of photovoltaic cell defects in electroluminescence images," *Energy*, vol. 189, Dec. 2019, Art. no. 116319.

XIONG ZHANG received the B.E. degree in electronic engineering and the M.E. degree in electronic circuit and system from the Taiyuan University of Technology, Taiyuan, China, in 1996 and 2003, respectively. Since 1996, he has been with the Taiyuan University of Science and Technology, where he is currently a Professor. His current research interests include multimedia communication, image/video processing, and pattern recognition.

TING HOU received the B.E. degree in electronic information engineering from the Taiyuan University of Science and Technology, Taiyuan, China, in 2019, where she is currently pursuing the M.E. degree with the Institute of Digital Media and Communication. Her research interests include image processing, object detection, and surface defects detection.

YAWEN HAO received the B.E. and M.E. degrees from the Taiyuan University of Science and Technology, Taiyuan, China, in 2017 and 2020, respectively. She is currently working with China Standard Software Company Ltd. Her research interests include image processing, object detection, and surface defects detection.

HONG SHANGGUAN received the B.E. degree in biomedical engineering and the Ph.D. degree in signal and information processing from the North University of China, in 2011 and 2016, respectively. Since 2016, she has been with Taiyuan University of Science and Technology, where she is currently an Associate Professor. Her research interests include medical image processing and pattern recognition.

ANHONG WANG received the B.E. and M.E. degrees in electronic information engineering from the Taiyuan University of Science and Technology (TYUST), in 1994 and 2002, respectively, and the Ph.D. degree from the Institute of Information Science, Beijing Jiaotong University, in 2009. She became an Associate Professor with TYUST, in 2005, and became a Full Professor, in 2009. She is currently the Director with the Institute of Digital Media and Communication, TYUST. She is also leading several research projects, including two National Science Foundations of China. She has published more than 100 articles in international journals and conferences. Her research interests include image/video coding and transmission, compressed sensing, and secret image sharing.

SICHUN PENG received the B.E. degree in electronic information engineering from the Taiyuan University of Science and Technology, Taiyuan, China, in 2018, where she is currently pursuing the M.E. degree with the Institute of Digital Media and Communication. Her research interests include image processing and surface defect detection.